TECHNOLOGY

A microfluidic biochip for complete blood cell counts at the point-of-care

U. Hassan[1,2,3], B. Reddy, Jr.[2,3], G. Damhorst[2,3], O. Sonoiki[1,2], T. Ghonge[2,3], C. Yang[4] & R. Bashir[2,3]

Complete blood cell counts (CBCs) are one of the most commonly ordered and informative blood tests in hospitals. The results from a CBC, which typically include white blood cell (WBC) counts with differentials, red blood cell (RBC) counts, platelet counts and hemoglobin measurements, can have implications for the diagnosis and screening of hundreds of diseases and treatments. Bulky and expensive hematology analyzers are currently used as a gold standard for acquiring CBCs. For nearly all CBCs performed today, the patient must travel to either a hospital with a large laboratory or to a centralized lab testing facility. There is a tremendous need for an automated, portable point-of-care blood cell counter that could yield results in a matter of minutes from a drop of blood without any trained professionals to operate the instrument. We have developed microfluidic biochips capable of a partial CBC using only a drop of whole blood. Total leukocyte and their 3-part differential count are obtained from 10 μL of blood after on-chip lysing of the RBCs and counting of the leukocytes electrically using microfabricated platinum electrodes. For RBCs and platelets, 1 μL of whole blood is diluted with PBS on-chip and the cells are counted electrically. The total time for measurement is under 20 minutes. We demonstrate a high correlation of blood cell counts compared to results acquired with a commercial hematology analyzer. This technology could potentially have tremendous applications in hospitals at the bedside, private clinics, retail clinics and the developing world.

Keywords: Cytometry; Microfluidic; Complete Blood Cell Counts; Point-of-Care; Coulter Counting.

INNOVATION

An automated and portable point-of-care blood cell counter capable of providing results in a matter of minutes from a blood drop (finger prick) could have tremendous impact in revolutionizing personalized health care in both the developing and the developed world. In this work, we have developed microfluidic biochips to count white blood cells (WBCs), three-part differential subtypes, red blood cells (RBCs) and platelets, using just 11 μL of whole blood in 20 minutes. The technology is based on purely electrical cell counting and does not require any fluorescent labels or manual off-chip pre-sample processing. We found a high correlation when our biochips cell counts were compared with the hematology analyzer counts from a clinical laboratory (Carle Foundation Hospital, Urbana, IL).

INTRODUCTION

The complete blood count (CBC) is among the most ubiquitous diagnostic tests in primary and acute care. For example, in acute radiation syndrome (ARS), a CBC test with leukocyte differentials is required for the rapid management of the disease[1]. In radiation and chemotherapy, the CBC is routinely performed to observe the necessary cells production by bone marrow to ensure the health of the patient. Inflammation, leukemia, tissue injury, bone marrow failure and immunodeficiency can all be identified by irregular leukocytes counts and their differentials. Similarly, bone marrow fibrosis, lymphoma, aplastic anemia and lupus erythematosus

are associated with abnormal platelet count. Excessive bleeding, kidney bleeding, cancer and mechanical trauma can be accompanied by changes in the RBCs count[1–3]. Thus, a microfluidic disposable and economical CBC test could help in monitoring all of these disorders at higher frequency, potentially enabling the diagnosis of diseases much earlier. CBC tests include counting of total WBCs, a five-part differential (lymphocytes, monocytes, neutrophils, basophils, eosinophils), RBCs, platelets and their indices (mean cell volume) and hemoglobin concentration. Most commercially available cell counting systems are flow cytometers or hematology analyzers[2–4]. The ubiquitous CBC is performed using automated hematology analyzers while flow cytometers are used for any specific cell counting (e.g., CD4+ T cells or CD8+ T cells for AIDS diagnostics or HIV management)[5].

Hematology analyzers can be both optical and electrical. In commercial systems, the infused blood is first split into two channels. The RBCs are then lysed in the WBC counting channel. In optical analyzers, a laser illuminates the cells as they pass through the flow cell in a single-file manner. The scattered light is collected by two photo-detectors. The scattered light collected by the photo detector in line with the laser is called forward scatter, and the scattered light collected by the photo-detector perpendicular to the laser is called backscatter. Forward scattered light determines the size of the cells and backscatter gives information on the membrane properties. The forward and backscatter plots allow us to differentiate total WBCs and their sub-types. In electrical hematology

analyzers, the blood cell counting is based on the cell size and membrane properties, which are probed by using kHz to MHz range frequencies with sensing electrodes.

A microfluidic device capable of enumerating the blood cells from a drop of blood could have tremendous applications ranging from clinical testing laboratories to point-of-care settings[6–9]. Microfluidic devices for cell counting have been reported using coulter counters and using AC signals[10–13]. Holmes et al. has shown the total leukocyte count and its differential using multi-frequency analysis[7]. Most of the above mentioned microfluidic counters were based on impedance cell counting technology[14,15]. Nguyen et al. have also characterized a biochip for CBC; however, the study lacks comprehensive differential counts, demonstrates only a small number of samples for statistical validation, and reports a small dynamic range of cell counts of blood samples[16]. Recently, Smith et al. have also shown an image-based device for complete blood cell counts with off-chip sample preparation[17]. However, the translation of their optical device to a portable system will have illumination non-uniformity and higher noise issues that they also mentioned in their article[17]. In our previous studies, we have also characterized in detail our microfluidic impedance sensors to count CD4 and CD8 T cells for HIV diagnostics using a differential capture technique[18,19]. We have also characterized the coincidence effects in our counter[20] and performed a detailed mathematical characterization of the electrical cell counting process[21].

In this current study, we report a comprehensive characterization of blood cell counting including total leukocytes and their three-part differentials, RBCs and platelet count. We demonstrate the operation of the device for a wider dynamic range of cell counts, including blood samples collected from patients admitted to a non-coronary Intensive Care Unit (ICU) at the Carle Foundation Hospital, Urbana, IL. The immune system of the ICU patients is often highly compromised and we were able to demonstrate a leukocyte dynamic range from as low as 200 cells/μL up to around 15,000 cells/μL. We also collected blood samples from cancer patients undergoing chemotherapy (anemic patients) and using our chip, we were able to show that these patients have significantly lower RBC and platelets counts when compared to healthy donor samples. Our blood cell counter exhibits the potential to improve patient care in a wide spectrum of medical settings.

METHODS AND MATERIALS

Experimental approach

A schematic illustrating the overall approach for a chip capable of WBC counts (three-part differential), RBC counts and platelet counts is shown in **Fig. 1**. We begin with a drop of blood typically around 50 μL in volume. From this, we meter out 11 μL of blood off-chip using an automated switching valve to input to the chips (**Supplementary Fig. 1**). Since electrical differentiation of the cells is primarily based on size differences, platelets and RBCs can be differentiated electrically, and the lymphocytes can be differentiated from other types of WBCs based on the observed pulse amplitude. Two separate

chips were used to obtain the three-part WBC differential and the RBC/platelet counts. For WBC counts, the infused blood is exposed to the lysing and quenching solutions to eliminate the RBCs from the solution. As shown in the top path in **Fig. 1**, the solution now contains a mix of WBCs, including neutrophils (60%), lymphocytes (30%), monocytes (7.5%), eosinophils (3%) and basophils (<0.5%). Since fewer than 10 basophils are present per μL of blood, basophils will not be counted and can be ignored for the proof of concept experiments. The solution is then flowed through the electrical counter of the chip, resulting in a count that contains lymphocytes, neutrophils, monocytes and eosinophils. At this point, a total lymphocyte count can be extracted since the lymphocytes can be separated based on their different pulse amplitudes. The remaining cells are grouped into a population consisting of neutrophils, monocytes and eosinophils. Neutrophils can be differentiated further from monocytes and eosinophils based on their membrane properties that is reflected by the impedance change at high frequencies (greater than 1 MHz)[22] (**Supplementary Fig. 2**).

For RBC and platelet counts (lower path in **Fig. 1**), a dilution of the blood is necessary because the concentration of RBCs is extremely high, i.e., about five million cells per μL in healthy human blood samples. The dilution factor will need to be optimized to maintain accurate counts without increasing the test time significantly. After dilution, the RBCs and platelets can be counted using the same counting electrodes due to their difference in size.

Electrode design for accurate cell differentiation

Electrode design is important to properly differentiate between different cell types, e.g., lymphocytes from granulocytes + monocytes. A schematic of the WBC counting chip is shown in **Fig. 2**. The microfabricated platinum electrodes are aligned within the 15 μm × 15 μm aperture cross-section[21]. Blue circles represent typical leukocytes. A schematic of the sensing region is shown in **Fig. 2b**. The red circle represents a leukocyte in the middle of the two electrodes. The output voltage of the sensing region is measured as A–B. The peak of the voltage 'A' will occur when the cell is exactly in the middle of the first two electrodes. Two relevant cases exist. In the first case, the spacing between the electrodes is greater than the cell diameter such that no portion of the cell is present over the second electrode, when the cell is in the middle of first two electrodes. The output voltage B will be zero in this case and the maximum pulse amplitude will be preserved. In the second case, the spacing between the electrodes is
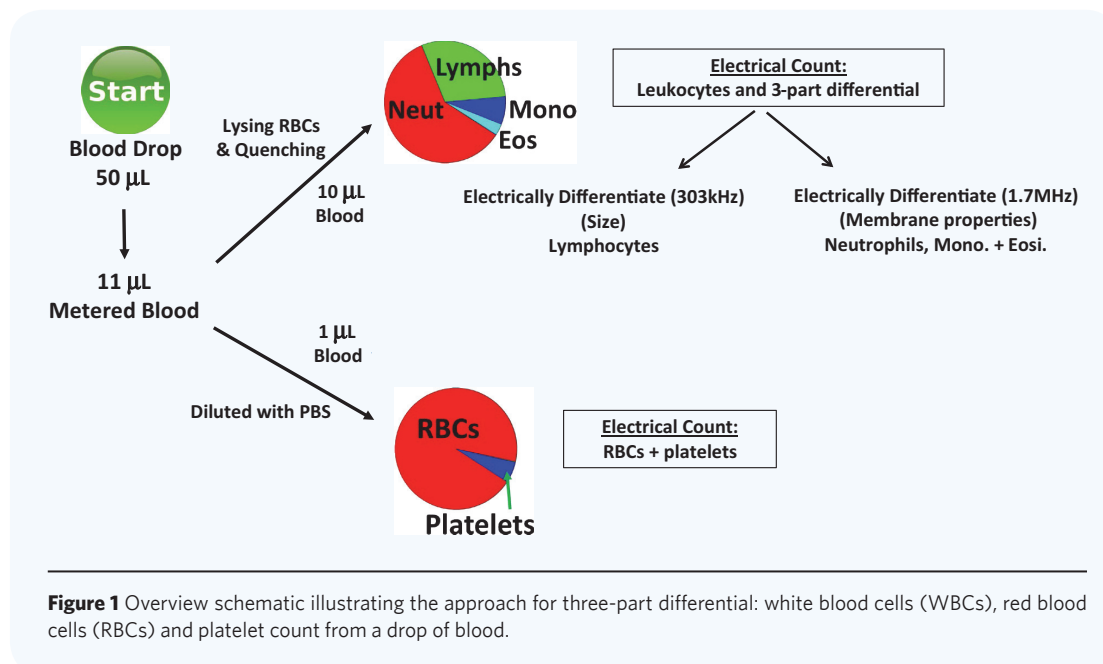

Figure 1 Overview schematic illustrating the approach for three-part differential: white blood cells (WBCs), red blood cells (RBCs) and platelet count from a drop of blood.
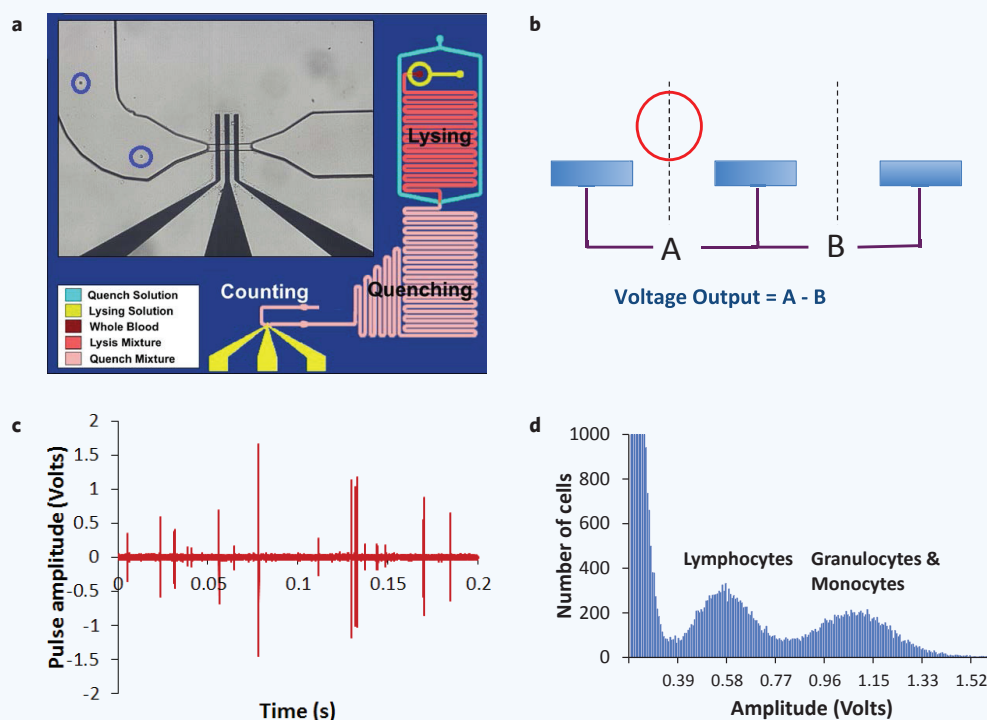
Figure 2 Differentiation between lymphocytes and granulocytes/monocytes. (**a**) Schematic of the leukocyte counting chip with lysing, quenching and counter modules shown in different colors. The image of the platinum microfabricated electrodes bonded and aligned to the coulter aperture of 15 μm × 15 μm is also shown as inset[21]. (**b**) Schematic of the sensing region. The red circle represents a leukocyte in the middle of the two electrodes. The peak of the voltage 'A' will occur when the cell is exactly in the middle of the first two electrodes. The spacing between the electrodes should be sufficiently large such that no portion of the cell is present over the second electrode, making B = 0. This will preserve the peak of the output voltage pulse (A–B) corresponding to cell size. (**c**) The typical voltage pulses obtained as the leukocytes pass through the counting region. (**d**) The amplitude histogram of the cell voltage pulses obtained with the sensing region consisting of the 15 μm spacing and width of the electrodes.

smaller than the cell diameter. When the cell is in the middle of first two electrodes, a portion of the cell will be over the second electrode, thus producing the output voltage B > 0. The resulting differential signal A–B will lose the maximum amplitude of the pulse that corresponds to the cell size. Thus, for differentiating between different cell types, the electrode spacing should be greater than or equal to the maximum cell diameter that needs to be differentiated.

In order to effectively differentiate between lymphocytes, granulocytes and monocytes, the electrode spacing should be at least 15 μm, as the diameter of the granulocytes/monocytes ranges from 12–15 μm. The pulses obtained as the leukocytes pass over the counting electrodes are shown in **Fig. 2c**. The amplitude of the pulse is proportional to the size of the cell. **Supplementary Fig. 3** shows the cell voltage pulse amplitude histogram obtained with the sensing region consisting of the 5 μm spacing and width of the electrodes. Electrode spacing is less than the size of the cells, resulting in less accurate cell differentiation between lymphocytes and granulocytes + monocytes. The cell voltage pulse amplitude histogram was obtained with a sensing region consisting of the 15 μm spacing and width of the electrodes (**Fig. 2d**). Electrode spacing is greater than the size of the cells, resulting in more accurate cell differentiation.

Reagents

- Lysing buffer: 0.12% (v/v) formic acid and 0.05% (w/v) saponin in DI.
- Quenching buffer: 21.1785% v/v 10 × PBS + 2.301 g of sodium carbonate in DI water.

- Blood is diluted with 1× PBS (pH = 7.4) at different dilution factors for RBC and platelet counting.

Blood sample acquisition

Blood samples were drawn from healthy donors via venipuncture through an Institutional Review Board (IRB) consent process. ICU blood samples were collected from the Carle Foundation Hospital and were brought to the Micro and Nanotechnology Laboratory at the University of Illinois at Urbana-Champaign for the cell counting experiments. The blood samples were collected in EDTA-coated BD vacutainers and were kept at room temperature on a rotisserie. Experiments were performed within 6 hours of blood draw.

Chip fabrication

The negative master mold of the fluidics regions, including lysing, quenching and counting, were created by patterning an SU8-50 negative photoresist on the Si wafer. The surface of the Si-mold was salinized using 3-mercapto-propyltrimethoxysilane[20,21]. A mixture of polydimethylsiloxane (PDMS) is mixed with the curing agent with a ratio of 10:1 and is poured on the Si-mold that is then cured for 30 minutes at 90°C. The platinum electrodes are fabricated by patterning the negative of the electrodes on a Glass/Pyrex wafer using LOR3A and S-1805 photoresists. CD-26 developer is then used to develop the wafers. An adhesion layer of 25-nm titanium is evaporated which is then followed by 75 nm of platinum deposition[20,21]. Wafer is kept in Microchem PG remover for 20 min at 70°C to remove the undesired metal.

Power analysis

Power analysis is used to determine the sample size required to get the desired statistical values. In order to get the correlation coefficient, $\rho = 0.9$ we selected an alpha level (two tailed) of 0.01 and power at 0.9. For $\rho = 0.9$, $Z_\alpha = 2.58$. However, $Z_b = 1.28$ for the desired 0.9 power level. The following equation is used to calculate the required sample size, which gives $N = 13$.

$$N = \frac{\left(Z_\alpha + Z_b\right)^2}{\frac{1}{4}\left[\log_e\left(\frac{1+\rho}{1-\rho}\right)\right]^2} + 3 \tag{1}$$

Equipment used

Lysing and quenching buffers are infused with an Eksigent Nanoflow LC pump with precise flow rates. Metered volume of the blood sample was loaded into the chips using a Rheodyne MHP7980-500-1 valve. Input voltage signal was fed to the microfabricated electrodes using Zurich Instruments HF2LI lock-in amplifier. The voltages difference between

the electrodes was obtained by using the Zurich Instruments differential preamplifier HF2CA. The output signal from the lock-in amplifier is sampled using the PCI-6351 DAQ card (National Instruments). A customized Matlab program is written to perform the data analysis.

RESULTS AND DISCUSSION

Total WBC and three-part differential count

Erythrocytes are lysed by infusing lysing buffer in the microfluidic biochip. After the erythrocyte lysis the cell debris tends to clump and make "debris ghosts" which result in clogging of electrical cell counting aperture of $15\,\mu m \times 15\,\mu m$. The debris clump also produces an appreciable change in impedance and would result in background baseline voltage noise. In our previous study, we found that greater quenching time of about 48 seconds results in providing the shear stress long enough to disassociate the erythrocyte debris clumps[18]. However, adding the 48-second step in the biochip would not only increase the size of the chip but also result in high fluidic resistance of the biochip. Saponin helps in dissociating the debris.

The blood was lysed on-chip with a blood:lysing ratio of 1.75:12. The lysing time was optimized for 9 seconds. The lysing process was halted as the quenching buffer composed of sodium carbonate and PBS is mixed with the solution. The blood to quenching ratio was then adjusted to 1.75:10. The prepared solution was passed through

the microfabricated platinum electrodes of 15 μm width and 15 μm spacing. The input signal to the electrodes was 7 V and 303 kHz is multiplexed with 1.7 MHz. The data were acquired at the sampling frequency of 500 kHz. The amplitude histogram of all the leukocyte voltage pulses is shown in **Fig. 3a**. It shows the distinct separation of the lymphocytes and granulocytes + monocytes. Voltage thresholds for cell counting were selected manually considering the minima in between debris and lymphocytes and lymphocytes and granulocytes + monocytes. We compared the biochip counts with the control count using 10 blood samples collected from patients admitted to the ICU (shown in red) and 13 blood samples from non-ICU donors (shown in blue). The comparison of the biochip total WBC counts with control counts is presented in **Fig. 3b**. There is a good correlation between the two methods with $R^2 = 0.95$ and with total WBC recovery of 68.35%. The comparison of biochip total lymphocyte count with the control count is shown in **Fig. 3c**. It also shows a good correlation between the two methods with $R^2 = 0.96$ and with total lymphocyte recovery of 71.83%. The comparison of biochip total granulocyte + monocyte count with the control count is presented in **Fig. 3d**. It shows a good correlation between the two methods with $R^2 = 0.96$ and with total granulocyte + monocyte recovery of 68.02%.

Precision studies of WBC and differential counting

Repeated experiments were performed from a single blood sample to measure the precision of our cell counting experiments. The precision
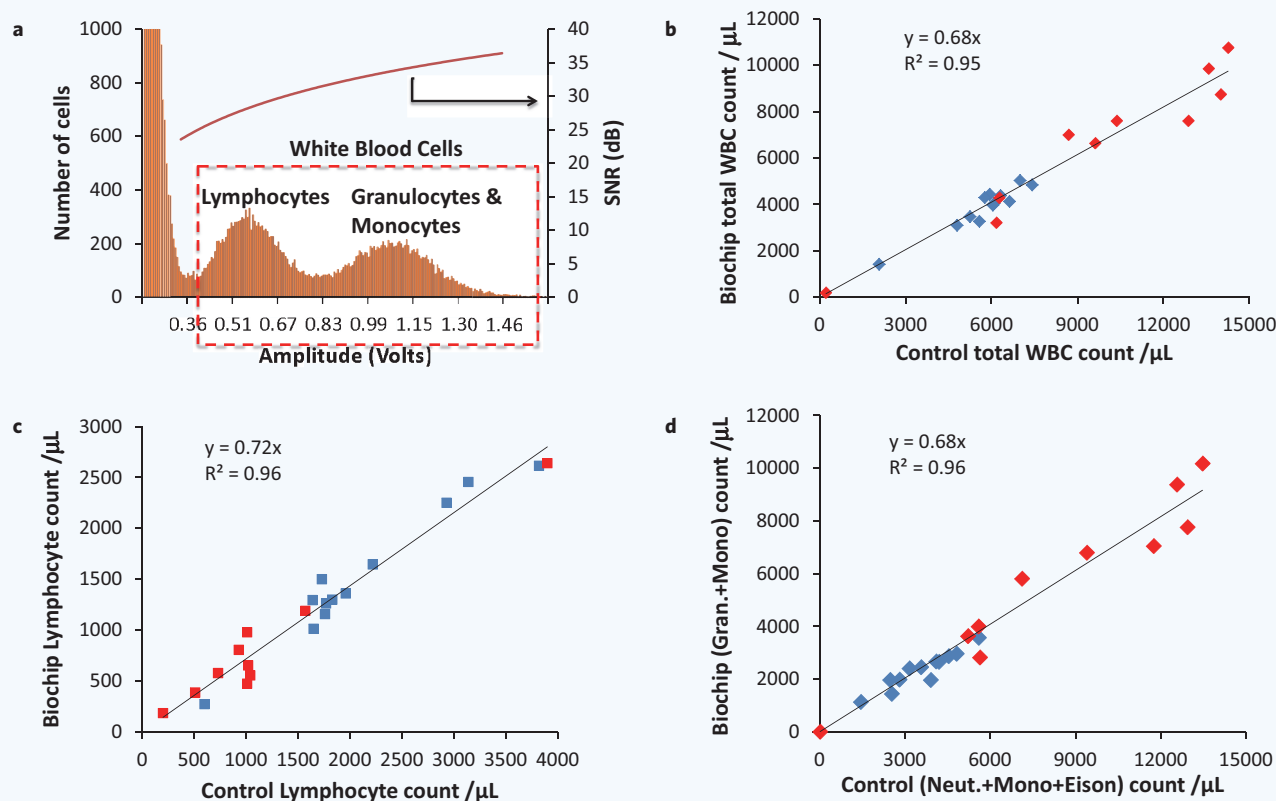

Figure 3 Comparison of biochip total leukocytes and their two-part differential (lymphocytes and granulocytes + monocytes) count from hematology analyzer control counts. Study is done on 23 blood samples with $n = 10$ collected from patients admitted to ICU (shown in red) and $n = 13$ from non-ICU donors (shown in blue). (**a**) Shows the histogram of the amplitude pulses for all the cells as they passed through the electrical counter. SNR of the leukocyte voltage pulses ranges from 25–37dB. (**b**) Comparison of biochip total WBC counts with the control count shows a good correlation with $R^2 = 0.95$. (**c**) Comparison of biochip total lymphocytes count with the control count shows a good correlation with $R^2 = 0.96$. (**d**) Comparison of biochip total granulocyte + monocyte count with the control count shows a good correlation with $R^2 = 0.96$.
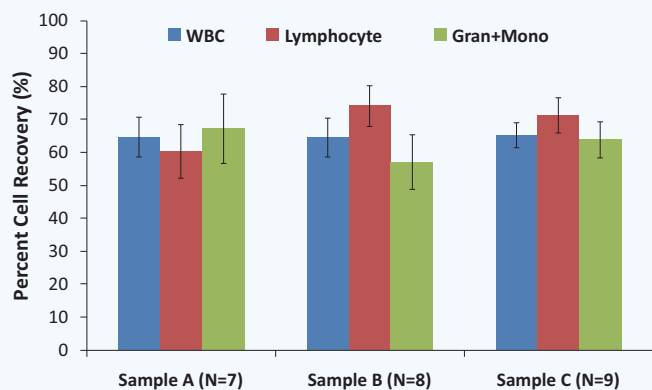
Figure 4 Precision studies for WBC, lymphocyte and granulocyte + monocyte counts from biochip in comparison with the control counts. The different-colored bars represent the mean and the error bars represent the std. of the cell recoveries for samples A, B and C with 7, 8 and 9 repeated experiments, respectively.

study for the total WBC, lymphocyte and granulocyte + monocyte counts from biochip in comparison with the control counts from the hematology analyzer is shown in **Fig. 4**. The different-colored bars represent the mean, and the error bars represent the standard deviation of the cell recoveries for samples A, B and C with 7, 8 and 9 repeated experiments, respectively.

Differentiating neutrophils from other granulocytes

To differentiate between neutrophils *vs.* monocytes + eosinophils, we fitted the lognormal distribution to the high frequency (1.7 MHz) histogram of the granulocyte + monocyte population as shown in **Supplementary Fig. 4**. Non-ICU samples were selected for this study. The skewness of the fitted lognormal distribution to the high frequency granulocyte + monocyte histogram is linearly correlated with the control monocyte + eosinophil concentration with an $R^2 = 0.83$ as shown in **Fig. 5a**. **Equation (2)** is used as a calibration to calculate the biochip monocyte + eosinophil concentration from the skewness of the fitted lognormal distribution to the high-frequency histogram of granulocyte + monocyte population. The comparison of the control monocyte + eosinophil count with the biochip's calculated monocyte + eosinophil using **Equation (2)** as a fit factor, is shown in **Fig. 5b**. This provides a good correlation with an $R^2 = 0.80$.

$$\left(Mono. + Eosi.\right)\frac{count}{uL} = 124.8\left(skewness\right) + 370.74 \qquad (2)$$
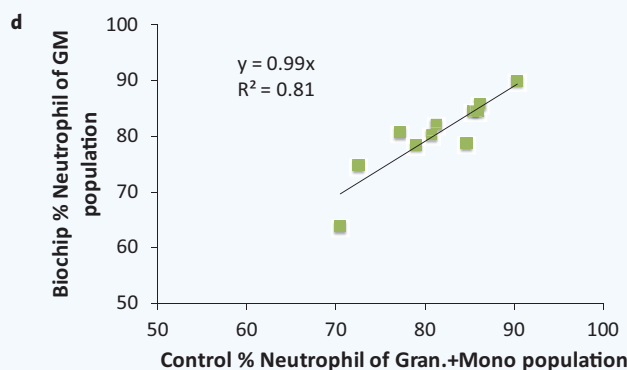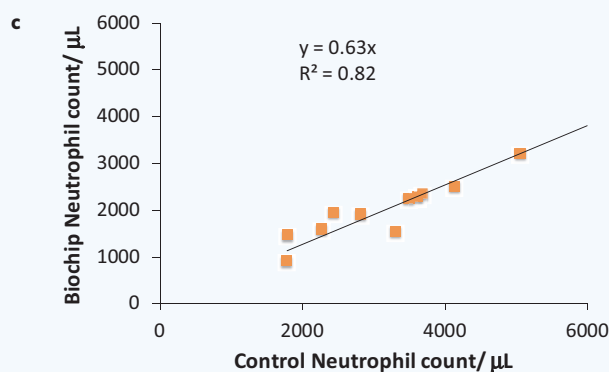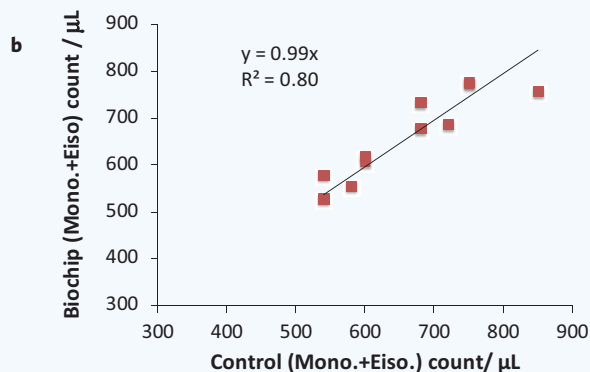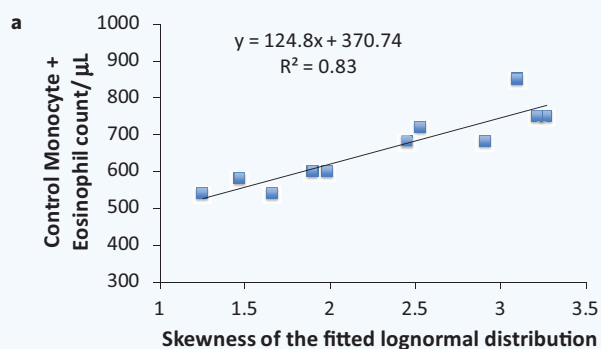

Figure 5 Differentiating neutrophils from monocytes and eosinophils. Non-ICU samples were selected for this study. (**a**) The skewness of the fitted lognormal distribution to the high-frequency granulocyte + monocyte histogram shows a linear correlation with the control monocyte + eosinophil concentration with an $R^2 = 0.83$. (**b**) Comparison of the control monocyte + eosinophil count with the biochip's calculated monocyte + eosinophil count ($R^2 = 0.80$). (**c**) Comparison of the control neutrophil count with the calculated biochip neutrophil count with $R^2 = 0.82$ and neutrophil recovery of 63.38%. (**d**) Comparison of the percent neutrophil of the granulocyte + monocyte concentration of the control with the calculated biochip percent neutrophil with $R^2 = 0.81$.

The biochip neutrophil count can be calculated with the following equation:

$$Biochip\,neutrophil\,count = low\,frequency\,(granulocyte + monocyte)$$
$$- count - 0.68\,(Biochip\,Mono. + Eosin.count),$$
$$(3)$$

where Biochip Mono. + Eosino. count were obtained from **Equation (2)** and 0.68 value represents the recovery of the total granulocyte + monocyte population with low frequency. The comparison of the control neutrophil count with the calculated biochip neutrophil count is shown in **Fig. 5c**. The biochip neutrophil count is calculated using **Equation (3)**. There is a good correlation with $R^2 = 0.82$ and neutrophil recovery of 63.38%.

The percentage of the total neutrophils comprising total granulocyte + monocyte should remain constant between control results and results calculated from biochip counts. The comparison of the neutrophil percent of the granulocyte + monocyte concentration from the control results with the calculated biochip neutrophil percentage is shown in **Fig. 5d**. There is a good correlation with $R^2 = 0.80$. To further validate neutrophil counts obtained from the skewness analysis, we performed a control experiment in which lysed blood output was collected from the biochip. The sample was conjugated with CD66b fluorescent antibody (this antibody is specific to the neutrophils). After running it from flow cytometer, the neutrophil population was gated on the fluorescent *vs.* side scatter plot (**Supplementary Fig. 5**). The resulting neutrophil counts were compared with our electrical neutrophil counts obtained from skewness analysis. The analysis was done for three samples and the % error obtained was 5.2%, 3.7% and 6.1% respectively.

Electrical counting of erythrocytes and platelets

Optimization of electronic settings and digital signal filtering

Platelets, being the smallest (~1–2 µm diameter) of all the blood cell types, are the most difficult to measure. To measure the platelets and the RBCs, the blood was diluted off-chip with PBS with a ratio of 1:300. The diluted blood was passed through the counting electrodes at 40 µL/min and the data was sampled at 1 Ms/sec. The sensing region of the counting electrodes was reduced to 5-µm spacing and width of electrodes with the same channel aperture of 15 µm × 15 µm resulting in higher sensitivity. The amplitude histogram of the voltage pulses obtained is shown in **Fig. 6**. We varied the voltage and gain settings to acquire the platelets signal. The amplitude histogram of the voltage pulses was obtained as the cells in the diluted blood are passed through the counting region (**Fig. 6a**). The input voltage is set to 5 V with a differential amplifier gain of 10. The red arrow shows the zoomed-in version of the black dotted rectangle, which shows a smooth decrease of RBC distribution. The histogram with the input voltage of 10 V and a differential amplifier gain of 10 was obtained (**Fig. 6b**). The zoomed-in version shows an appearance of platelet distribution to the left of the RBC distribution. A typical voltage pulse corresponding to the RBC is shown in **Fig. 7** with signal-to-noise ratio (SNR) of 21.7 dB. A typical voltage pulse corresponding to the platelet with an SNR of 11.4 dB is shown in **Fig. 7**. In order to obtain the maximum SNR for the pulses, the input voltage to the electrodes is varied from 1–10 V. **Supplementary Fig. 6** shows the corresponding increase in the mean SNR of the RBC pulses with the increase in the input voltage. It shows a linear increase with an R^2 value of 0.86.

The frequency spectrum of the cell counting experiment data will allow us to observe the noise components in the frequency domain. **Supplementary Fig. 7** shows the frequency spectrum of the entire cell counting data without performing any digital filtering. There is low-frequency noise in the data because of the baseline drifts, electronic noise and power-line interference (60 Hz). Most of the cells pulses spectrum lies in the range of 5–90 kHz as shown in **Supplementary Fig. 7a**. There is an input frequency noise of 303 kHz and another high-frequency noise at 314.8 kHz as shown in **Supplementary Fig. 7b**. These can be removed by using a low-pass filter with cut-off-frequency less than 303 kHz.

The low-frequency noise in the data is removed by applying a high-pass filter with cut-off frequency of 20 Hz. To remove the power line frequency, a band-stop filter is used with cut-off frequencies of (58, 62) Hz. The second harmonic of the power line frequency is also removed using a band-stop filter with cut-off frequencies of (118, 122) Hz. The baseline drift is also corrected. The frequency spectrum of the cell counting experiment data after signal filtering is shown in **Supplementary Fig. 8**.

RBC and platelet counting with off-chip dilution

The erythrocyte (RBC) concentration in the blood sample is significant and thus requires dilution for accurate cell counting. The RBCs can be
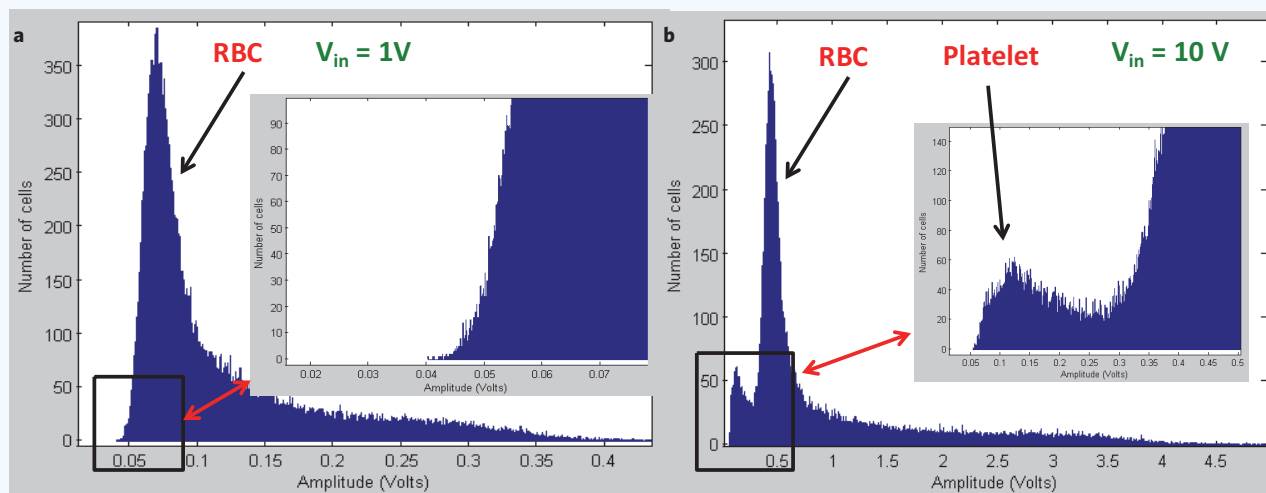

Figure 6 The amplitude histograms of the voltage pulses obtained as the cells in the diluted blood (blood:PBS = 1:300) is passed through the counting channel. (**a**) The input voltage is 5 V with a differential amplifier gain of 10. The red arrow shows the zoomed-in version of the black dotted rectangle, which shows a smooth decrease of RBC distribution. (**b**) The input voltage is 10 V with a differential amplifier gain of 10. The zoomed-in version shows an appearance of platelet distribution to the left of the RBC distribution.
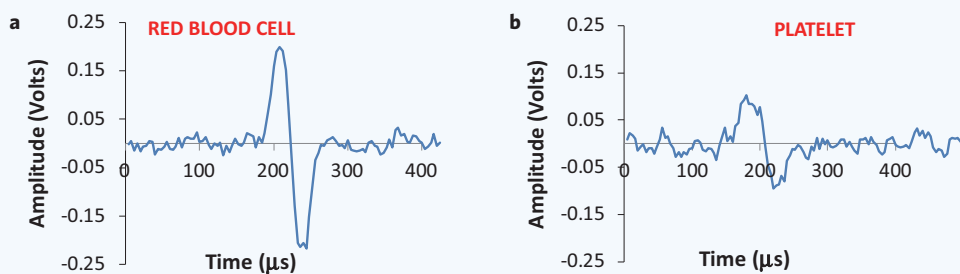
Figure 7 (**a**) A typical voltage pulse of an RBC with a signal-to-noise ratio (SNR) of 21.7 dB. (**b**) A typical voltage pulse of a platelet with an SNR of 11.4 dB.

Blood is diluted with PBS with a ratio of 1:200 and flowed at 40 µL/min through the electrical counter. The precision results of RBC-counting are shown in **Fig. 9a**. '1' shows the healthy donor sample with a CV = 2.6% for five repeated experiments; '2' shows a cancer donor sample with a CV = 5.5% for five repeated experiments; and '3' shows another cancer donor sample with a CV = 5.8% for four repeated experiments. The precision results of RBC-counting are shown in **Fig. 9b**. '1' shows the healthy donor sample with a CV = 10.2% for five repeated experiments; '2' shows a cancer donor sample with a CV = 8.1% for five repeated experiments; and '3' shows another cancer donor sample with a CV = 9.3% for four repeated experiments.

differentiated from platelets and WBCs from the electrical voltage pulse's amplitude histogram as the RBC is bigger than a platelet but smaller than a WBC. The blood samples were diluted off-chip with different blood:PBS dilution ratios. We flowed the diluted blood sample through our impedance cell counter and count all the pulses; the sample contains RBCs, platelets and all WBCs. The leukocytes comprise about 0.5% and platelets about 3–5% of the erythrocytes, and after dilution the leukocyte concentration in the sample becomes very low — around 50 cells/µL, resulting a negligible effect on the counting results. The control RBC counts were compared with the counts obtained from the biochip using 22 blood samples (**Fig. 8a**). Blood is diluted with PBS at different dilutions (PBS:blood) and flowed through the biochip. It shows a good correlation between the two methods with $R^2 = 0.96$ and the cell recovery of 96.35%. The cases for which the biochip noise is higher; platelet distribution did not appear. The noise comparison of the biochips for platelet counting is given in 'Discussion' section. The control platelet counts were compared with the counts obtained from the biochip using 13 blood samples (**Fig. 8b**). It shows a good correlation in between the two methods with $R^2 = 0.84$ and the cell recovery of only 51%. The decrease in the cell recovery can be associated with the high noise in the biochip, resulting in loss of platelet pulses in the noise. Platelets, being the smallest (~1–2 µm diameter), result in small impedance change.

Precision studies of RBC and platelet counting

Repeated experiments were performed from a single blood sample to measure the precision of our RBC- and platelet-counting experiments.

RBC and platelet counting with on-chip dilution

The on-chip dilution is performed on the biochip; the schematic is shown in **Fig. 10**. The PBS and the blood are infused in the biochip at the indicated inlet ports. The PBS is mixed with blood at the ratio of 40:0.5 µL/min in the serpentine channels. The electrical counter counted the cells in the diluted blood as they pass through the electrodes. In order to improve the SNR the width and spacing of the electrodes was reduced to 5 µm.

The Blood is diluted on-chip with PBS with flow rate ratio (blood: PBS = 0.5:40 µL/min). The resulting diluted blood is flowed through the electrical counter. The control RBC counts are compared with the counts obtained from the biochip using 21 blood samples (**Fig. 11a**). It shows a good correlation between the two methods with $R^2 = 0.82$ and the cell recovery of 93.52% after coincidence correction. The decrease in the cell recovery can be associated with the high number of coincidences at the low dilution factor. The control platelet counts are compared with the counts obtained from the biochip using 13 blood samples (**Fig. 11b**). It shows a good correlation between the two methods with $R^2 = 0.90$ and the cell recovery of 67.85%. The decrease in the cell recovery can be associated with the high number of coincidences at the low dilution factor and loss of the platelets pulses in the noise.
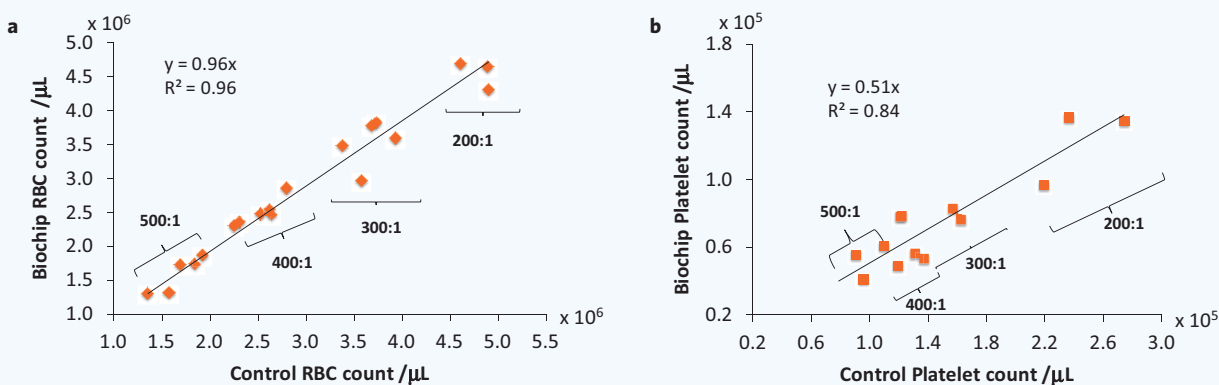

Figure 8 Erythrocyte and platelet counting. Blood is diluted with PBS at different dilutions (PBS:blood) off-chip and flowed through the biochip. (**a**) Comparison of the control RBC counts with the counts obtained from the biochip using 22 blood samples with $R^2 = 0.96$. (**b**) Comparison of the control platelet counts with the counts obtained from the biochip using 13 blood samples with $R^2 = 0.84$.
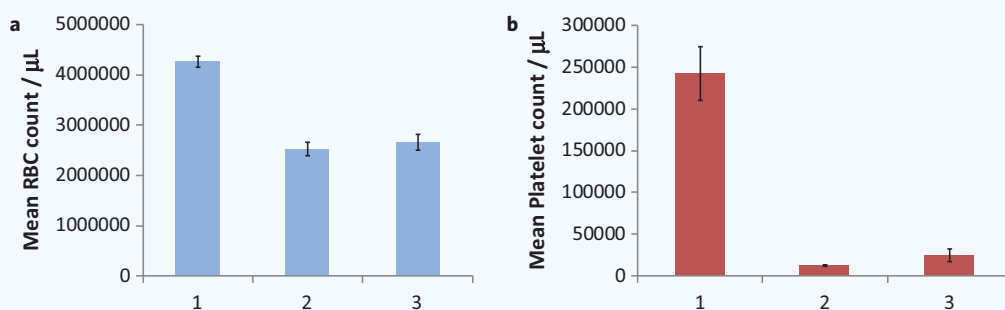
Figure 9 (**a**) Precision studies of RBC counting. '1' shows the healthy donor sample with a CV = 2.6% for five repeated experiments; '2' shows a cancer donor sample with a CV = 5.5% for five repeated experiments; and '3' shows the cancer donor sample with a CV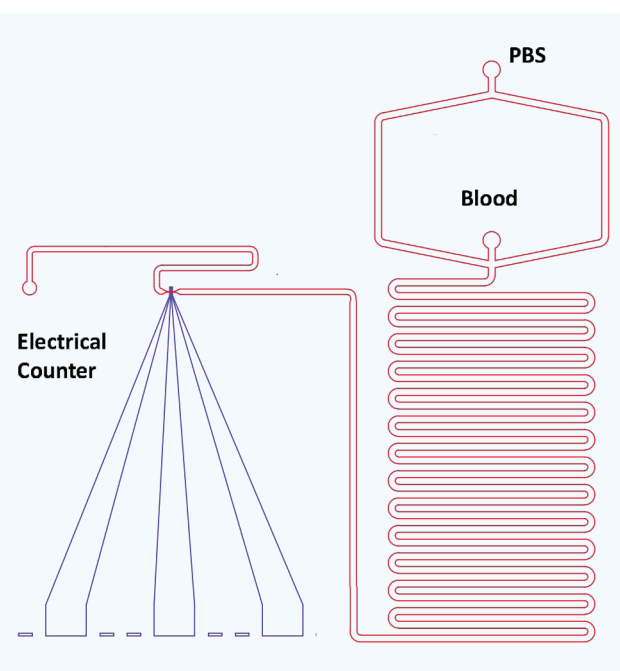 = 5.8% for four repeated experiments. (**b**) Precision studies of platelet counting. '1' shows the healthy donor sample with a CV = 10.2% for five repeated experiments; '2' shows a cancer donor sample with a CV = 8.1% for five repeated experiments; and '3' shows the cancer donor sample with a CV = 9.3% for four repeated experiments.

Figure 10 Schematic of the RBC- and platelet-counting biochip. PBS is mixed with blood at the ratio of 40:0.5 in the serpentine channels. The electrical counter counted the cells in the diluted blood as they passed through the electrodes.

DISCUSSION

Our sensor has the potential to be translated to a commercial point-of-care CBC biochip. However, being in early stages of development, there is much room to further improve the parameters including cell recovery, voltage thresholds for cell counting, electrodes configuration and skewness analysis for more sensitive and accurate results. Currently, threshold selection for the cell counting is performed manually while considering the minima between different populations. However, in a portable and completely automated CBC counter, this can be done using an automated algorithm considering two parameters, i.e., minima in between two distributions and a preselected threshold value which will be much more precise in mass manufactured cartridges and electrodes. The variability in the biochip fabrication in the current research settings can

be a limitation when it comes to achieving consistent properties and geometries of the electrodes. For example, the variability in the selected threshold value for total WBC counting was approximately 30% (Supplementary Information). In point-of-care automated cell counters, the threshold selection can be automated since the cartridges/electrodes will be commercially manufactured and the fabrication process is expected to be more consistent and streamlined.

Microfluidic biochips utilize an aggressive lysing step to ensure the lysing of the RBCs as the desired time to perform this lysing should be small. Hematology analyzers use lysing reagents that result in lysing/quenching time in the order of 10 minutes. In point-of-care microfluidic biochips, using these regents with significant higher times will result in unacceptably large assay time and use of extra reagent volumes. This will also result in a much higher footprint of the device, thus directly affecting the cost per assay. However, with our rapid lysing solution to effectively lyse all erythrocytes and to ensure the complete dissociation of RBC debris clumps (to prevent clogging of the chips; one of major problem in point-of-care biochips), the lysing solution resulted in loss of leukocytes as well.

In experiments for which we were able to see the platelet distribution; the standard deviation of the noise was less than 0.03 V. The baseline drift in the signal also got completely removed after the filtering and baseline correction algorithm as shown in **Supplementary Fig. 9**. However, for the experiments for which we were not able to see the platelet distribution, the standard deviation of the noise in the biochip is greater than 0.05 V. Also the baseline drift was very large compared to the good chips as shown in **Supplementary Fig. 10**.

The signal averaging technique can be used to improve the SNR that only works if the noise is Gaussian white noise and not pink or brown noise having spectral characteristics of $1/f$ and $1/f^2$, respectively. We have shown the decrease in the standard deviation of chip noise with signal averaging. PBS is flowed through the electrical counter at 40 μL/min and the chip noise is recorded. The measured standard deviation of the chip noise was 0.0873 V. **Supplementary Fig. 11** shows the decrease in the standard deviation of the chip noise with signal averaging. Increased number of samples for averaging will result in decreased standard deviation for the chip noise. After averaging with two samples, the standard deviation is reduced to about 0.06 V, which further decreased to 0.04 V after signal averaging with three samples. Platelets are 1–2 μm in size as compared to the channel cross-section of 15 μm × 15 μm. Any platelets flowing at the top of the channel might get lost in noise. This can be remedied by using hydrodynamic focusing[23]. For this we need to redesign the channel accordingly or introduce another buffer, which will not be desirable for a point-of-care device, where one objective is to minimize the number of reagents.

After performing the high-pass filtering at 20 Hz and power-line filtering at 60 and 120 Hz, the frequency spectrum of the RBC, platelet counting experimental data with the sampling rate of 1 MHz and input signal frequency of 303 kHz are obtained and shown in **Fig. 6**. The red arrow shows voltage pulse frequency spectrum. The green arrow shows a peak at 303 kHz, which can be further removed to decrease the chip's noise. A low-pass filter of 200 kHz can be used to remove this noise. The standard deviation of the chip noise without using this filter
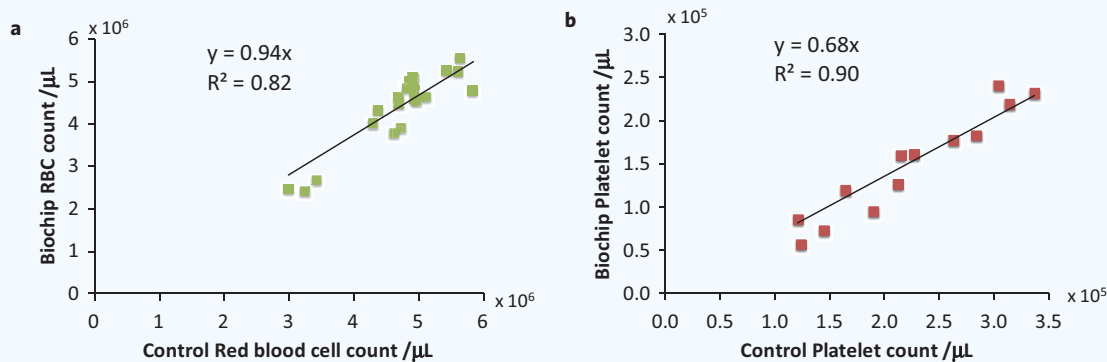
Figure 11 Erythrocyte- and platelet-counting experiments with on-chip blood dilution. Blood is diluted on-chip with PBS with flow rate ratio (blood: PBS = 0.5:40 μL/min) and flowed through the biochip. (**a**) Comparison of the control RBC counts with the counts obtained from the biochip using 21 blood samples with $R^2 = 0.82$ and the cell recovery of 93.52%. (**b**) Comparison of the control platelet counts with the counts obtained from the biochip using 13 blood samples with $R^2 = 0.90$ and the cell recovery of 67.85%.

was 0.0564 V, which decreased to 0.0305 V after low-pass filtering was performed on the data with cut-off frequency of 200 kHz.

Holmes *et al.* were able to isolate the granulocytes from monocytes with top-bottom electronic configuration that is more sensitive than our co-planar electrodes configuration[7]. However, top-bottom electrodes configuration may impose some developmental challenges like alignment of electrodes within a few microns and electronic connectors arrangements from both layers, resulting in more complicated and potentially expensive cartridges.

The blood samples collected from the ICU patients sometimes have abnormally high number immature granulocytes ranging from 10–2,200 cells/μL as compared to 10–20 cells/μL in healthy samples. The high number of immature granulocytes will result in changing the skewness level of the fitted lognormal distribution. Thus, the regular correlation of skewness with the control monocyte + eosinophil count does not hold with high number of immature granulocytes. When we fitted bimodal distributions to the impedance histograms at high frequency (using maximum likelihood optimization for parameter estimation in Matlab), the fitting function was unable to converge or produced erroneous fitting values for cases where the monocytes population was less than <10% of leukocytes. Our results were obtained for monocytes + eosinophils population comprising of 8.5–16% of total leukocytes.

RBC recovery is significantly higher in our biochip; however WBC recovery of ~65% is acceptable only if the precision of the test is good, and the percent recovery can be used as a correction factor to get the accurate counts[24]. However, for platelet counts we do realize that currently the recovery is low, i.e., ~50–60%. This can be further improved by various techniques as we discussed above. Also, the current work presents two separate chip modules for RBC/platelet counting and WBCs and its differential counting. However, both of these modules can be easily integrated into a single cartridge. For research purposes, the split modules allowed us to characterize, debug and run experiments in a detailed fashion.

The experiments were performed with different patient populations and over a large dynamic range. The standard deviation in the recoveries of WBCs, lymphocytes and granulocytes + monocytes we obtained were 8.12%, 13.11% and 8.89%, respectively. The variability in recovery of cell counts can be attributed to many factors including the uncontrolled temperature and humidity environment of our experiments, variability in the fabrication of cartridges that result in different SNR measurements from the setup, etc. In addition, there can be an inherent variation in cell counts across different instruments from same manufacturers. The current variability in the recovery results can be further reduced with more standardized processes

of fabrication and a controlled environment in a point-of-care counter.

The applied voltage used in the erythrocyte counting experiments is up to 10 V. The electrolysis of the cells depends on many factors including applied voltage and whether it is DC or AC, the frequency of the applied voltage, flow rate of the cells and the critical time for irreversible electroporation[25–27]. If the actual transmembrane voltage increases well above 1 V, then electroporation can begin to happen[25]. In our experimental conditions, with 10-V peak voltage at frequency of 303 kHz, and using intracellular resistivity reported in literature, the resulting transmembrane potential can be calculated to be around 2 V. So looking at transmembrane potential only, we would be above the critical voltage to cause cell lysing. However, the electroporation (and irreversible electroporation and cell lysing) is also critically dependent on the time that the cells are exposed to the electrical field. The reported critical time for electrical lysis of erythrocytes can vary anywhere between 100 μs to a few milliseconds[25]. In our case, with the flow rates used in our experiments, the pulse width across two electrodes is approximately 50 μs. During this 50 μs, the cell is exposed to different electric field strengths at different times during the flow path over the electrodes. However, electroporation might have happened to the erythrocytes resulting in damaging the cell membranes. Hence, it is certainly likely that the SNR increase is not only due to increased voltage itself, but also due to electroporation or partial cell lysis resulting from the increased electric field. It however does not cause an error in the cell counting, which is the primary goal of our paper.

A portable CBC device exhibits the potential to improve patient care in a complete spectrum of settings. One of the most compelling possibilities is in resource-limited settings where laboratory tests are often inaccessible due to cost, poor laboratory facilities and the difficulty of follow-up upon receiving results that take days to process. Ease-of-use and the ability to interface with mobile communication devices such as smartphones and tablets with wireless internet connectivity enable a point-of-care device by which rapid results can be transmitted to a provider anywhere in the world, eliminating the need for a highly trained professional at the site of care and thus reducing the cost.

The wireless delivery of results to healthcare providers also enables use of the device in the home setting, particularly for patients with chronic conditions or those undergoing continued therapy that requires the monitoring of any one or multiple components of a CBC and WBC differential. Rapid results in a portable device carried on an ambulance will shape interventions in pre-hospital care and provide receiving emergency departments with CBC results upon arrival. When transport time is significant such as in rural settings, the CBC can provide an assessment of patient stability and can provide information to advise emergency medical technicians on further care.

In the emergency department, a rapid CBC device promises faster results than the current capabilities of clinical laboratories and will decrease laboratory workload. It not only may speed up life-saving care

in emergent cases, but also may improve emergency room throughput and ultimately decrease waiting time in busy hospitals. Upon a patient's admission to full hospital care, this device can be used at the bedside to monitor the patient regularly in the hospital room, especially a patient in an ICU. Finally, this device can be used in the physician's office during regular visits for basic screenings or follow-up examinations that require blood counts to be performed.

REFERENCES

1. Wallach, J. *Interpretation of Diagnostic Tests*, 7th ed. (Lippincott Williams & Wilkins, 2000).
2. CLIAwaived. *CBC (Hematology) Systems* (2003), http://www.cliawaived.com/web/CBC_(Hematology)_Systems.htm
3. Hassan, U. Microfluidic sensor for white blood cell counting and flow metering. M.S., Electrical & Computer Engineering, University of Illinois at Urbana-Champaign (2013).
4. Coulter, W.H. "Means for counting particles suspended in a fluid," US Patent 2656508 (1953).
5. Invitrogen. *Flow Cytometry Tutorials: Introduction* (2012), http://probes.invitrogen.com/resources/education/tutorials/4IntroFlow/player.html
6. Koch, M., Evans, A. & Brunnschweiler, A. Design and fabrication of a micromachined coulter counter. *J. Micromechan. Microeng.* **9**, 159–161 (1999).
7. Holmes, D., Pettigrew, D., Reccius, C.H., Gwyer, J.D., Berkel, C. & Holloway, J. Leukocyte analysis and differentiation using high speed microfluidic single cell impedance cytometry. *Lab Chip* **9**, 2881–2889 (2009).
8. Watkins, N.N., Sridhar, S., Cheng, X., Chen, G.D., Toner, M., Rodriguez, W.A. & Bashir, R. Microfabricated electrical differential counter for the selective enumeration of CD4+ T lymphocytes. *Lab Chip* **11**, 437–447 (2011).
9. Cheng, X., Liu, Y., Irimia, D., Demirci, U., Yang, L. & Zamir, L. Cell detection and counting through cell lysate impedance spectroscopy in microfluidic devices. *Lab Chip* **7**, 746–755 (2007).
10. Ellappan, P. & Sundararajan, R. A simulation study of the electrical model of a biological cell. *J. Electrostat.* **63**, 297–307 (2005).
11. Schoenbach, K.H., Katsuki, S., Stark, R.H., Buescher, E.S. & Beebe, S.J. Bioelectrics—new applications for pulsed power technology. *IEEE Trans. Plasma Sci.* **30**, 293–300 (2002).
12. Hughes, M.P. AC electrokinetics: Applications for nanotechnology. *Nanotechnology* **11**, 124–132 (2000).
13. Gawad, S., Schild, L. & Renaud, P. Micromachined impedance spectroscopy flow cytometer for cell analysis and particle sizing. *Lab Chip* **1**, 76–82 (2001).
14. Pierzchalski, A., Hebeisen, M., Mittag, A., Berardino, M.D. & Tarnok, A. Label-free single cell analysis with a chip-based impedance flow cytometer. *Proc. SPIE* **75681B**, (2010).
15. Cheung, K.C., Berardino, M., Schade-Kampmann, G., Hebeisen, M., Pierzchalski, A. & Bocsi, J. Microfluidic impedance-based flow cytometry. *Cytometry Part A* **77A**, 648–666 (2010).
16. Nguyen, J., Wei, Y., Zheng, Y., Wang, C. & Sun, Y. On-chip sample preparation for complete blood cell count from raw blood. *Lab Chip* **15**, 1533–1544 (2015).
17. Smith, Z.J. *et al*. Single-step preparation and image based counting of minute volumes of human blood. *Lab Chip* **14**, 3029 (2014).
18. Watkins, N.N., Hassan, U., Damhorst, D., Ni, H., Rodriguez, W. & Bashir, R. Microfluidic CD4+ and CD8+ T lymphocyte counters for point-of-care HIV diagnostics using whole blood. *Sci. Trans. Med.* **5**, 214ra170 (2013).
19. Hassan, U., Watkins, N., Edwards, C. & Bashir, R. Flow metering characterization within an electrical cell counting microfluidic device. *Lab Chip* **14**, 1469 (2014).
20. Hassan, U. & Bashir, R. Coincidence detection of heterogeneous cell populations from whole blood with coplanar electrodes in a microfluidic impedance cytometer. *Lab Chip* **14**, 4370–4381 (2014).
21. Hassan, U. & Bashir, R. Electrical cell counting process characterization in a microfluidic impedance cytometer. *Biomed. Microdevices* **16**, 697–704 (2014).
22. Ellappan, P. & Sundararaian, R. A simulation study of a electrical model of a biological cell. *J. Electrostat.* **63**, 297–309 (2005).
23. Watkins, N.N., Venkatesan, B.M., Toner, M., Rodriguez, W. & Bashir, R. A robust electrical microcytometer with 3-dimensional hydrofocusing. *Lab Chip* **9**, 3177–3184 (2009).
24. Dadgar, D., Burnett. P.E., Choc. MG., Gallicano. K. & Hooper, J.W. Application issues in bioanalytical method validation, sample analysis and data reporting. *J. Pharm. Biomed. Anal.* **13**, 89–97 (1995).
25. Morshed, B.I., Shams, M. & Mussivand, T. Electrical lysis: Dynamics revisited and advances in on-chip operation. *Crit. Rev. Biomed. Eng.* **41**(1), 37–50 (2013).
26. Joshi, R.P. & Schoenbach, K.H. Electroporation dynamics in biological cells subjected to ultrafast electrical pulses: A numerical simulation study. *Phys. Rev. E.* **62**, 1025–1033 (2000).
27. Salm, E., Jokilaakso, N., Chen, A., Millet, L., Guevara, C.D., Karlström, A.E., Sooryakumar, R. *et al*. Single cell manipulation and ultra localized cell lysis using silicon nanowires. *Lab Chip* **13**, 336–339 (2013).

## SUPPLEMENTARY INFORMATION

Volume metering

Supplementary Fig. 1 shows the volume metering method used to meter and flow a specific desired blood volume into the biochip. An Eksigent HPLC system is used to pump the reagents at the specific flow rates. Lysing and quenching reagents are directly infused into biochip at their respective inlet ports. An injection valve (two-position, six-port) connected to 10 µL tubing (volume of tube is adjusted to required volume) is used to meter out the desired blood volume. In first step, blood is infused into the measurement tubing; it fills it up and goes to the waste (path 'a'). During second step, the valve is switched to path 'b' electronically and PBS starts to push the metered blood into the biochip. The volumes of the tube used for white blood cells (WBCs), its differential counting and red blood cells (RBCs), platelet counting are 10 and 1 µL, respectively.
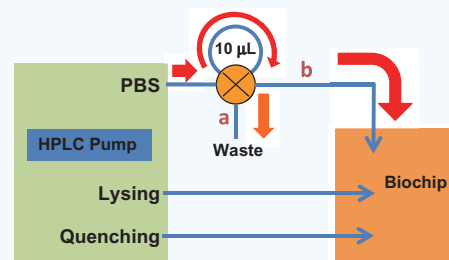

Supplementary Figure 1 Schematic of blood volume metering method for a WBC and its differential counting experiment. The volume of the measurement tube will be 1 µL for RBC/platelet-counting experiment.
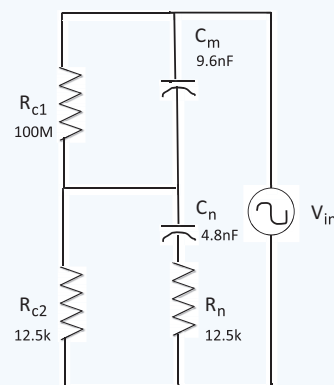

Supplementary Figure 2 The simplified electrical model of a cell.[22]
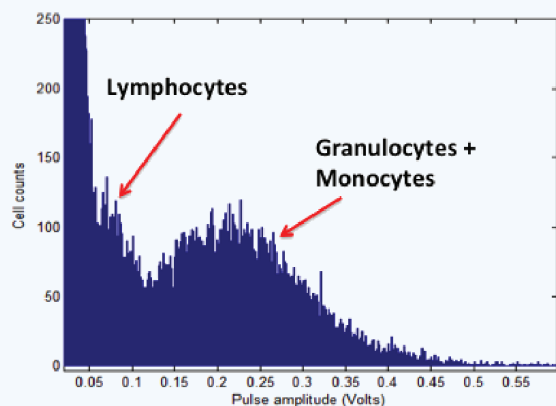
Supplementary Figure 3 The cell voltage pulse amplitude histogram obtained with the sensing region consisting of 5-µm spacing and width of the electrodes. Electrode spacing is less than the size of the cells, resulting in less accurate cell differentiation.
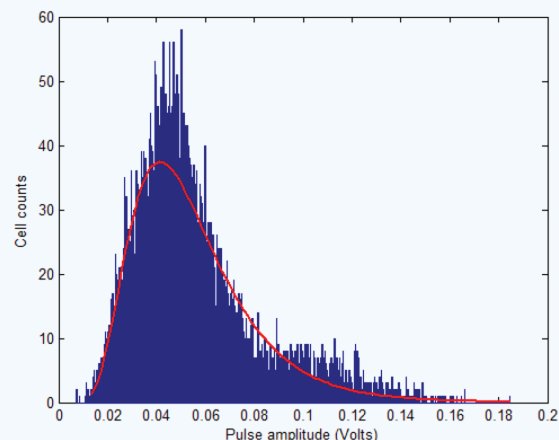
Supplementary Figure 4 The amplitude histogram of the voltage pulses obtained at high frequency of 1.7 MHz for the granulocyte + monocyte population. The distribution is fitted with the lognormal distribution.
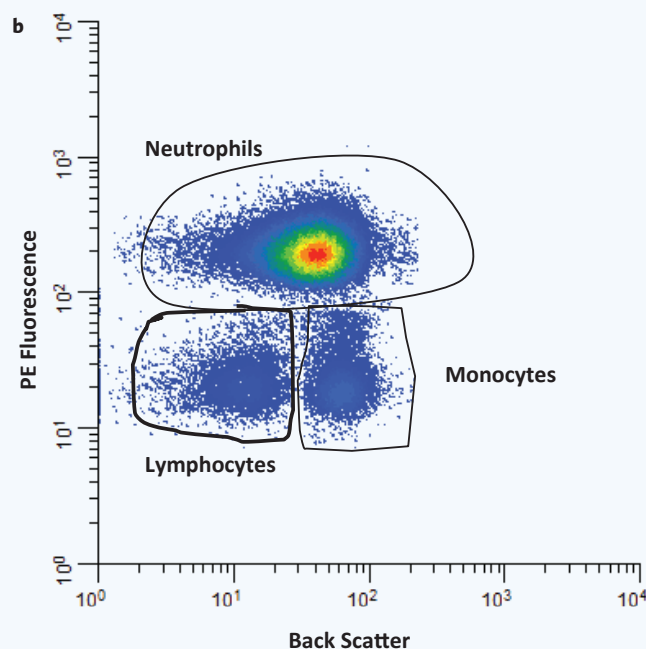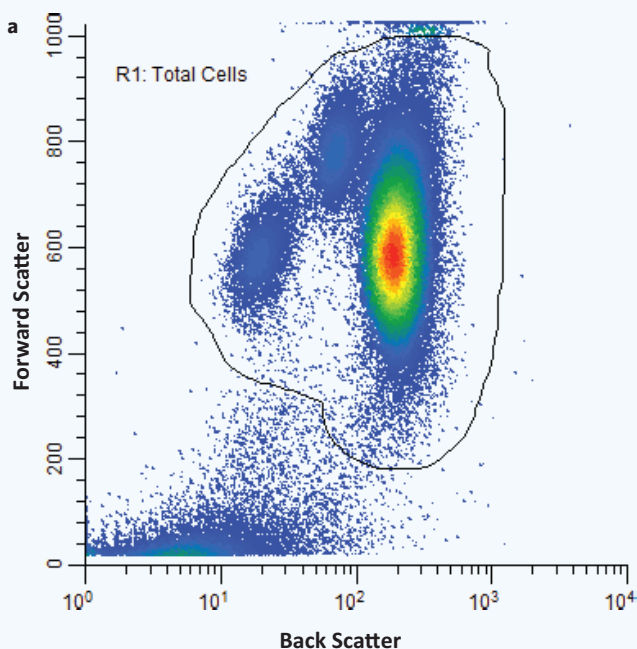
Supplementary Figure 5 Scatter plots when the lysed blood output of biochip ran through the flow cytometer. (**a**) Forward and backscatter plot shows the clear differentiation between total white blood cells (WBCs) and debris. (**b**) The scatter plot between (PE) channel and backscatter. Neutrophil population is gated and the gated counts were compared with the counts obtained from the skewness analysis.

Theoretical analysis

Supplementary Fig. 2 shows the electrical model of the cell. R_{c1} is the resistance of the plasma membrane (100 MΩ), which is highly resistive to the flow of charges. C_m is the capacitance of the plasma membrane. R_{c2} is the resistance of the cytoplasm, which comes in contact with the nucleus with nucleoplasm resistance, R_n. The capacitance of the nuclear membrane is represented by C_n and is approximately half of the membrane capacitance, since it is composed to two lipid bilayers.

At low frequencies, the input voltage appears at the plasma membrane, due to the plasma membrane resistance. At frequencies of about 100 kHz,

the impedance change is based on the cell size, since at these frequencies cells behave as a non-conducting fluid. At frequencies greater than 1 MHz, the change in impedance is based on different structural properties of the plasma membrane. At frequencies higher than 100 MHz, the change in impedance is based on the nuclear membrane properties. Thus, cells can be differentiated based on their sizes, plasma membrane and nuclear membrane structures.[22]
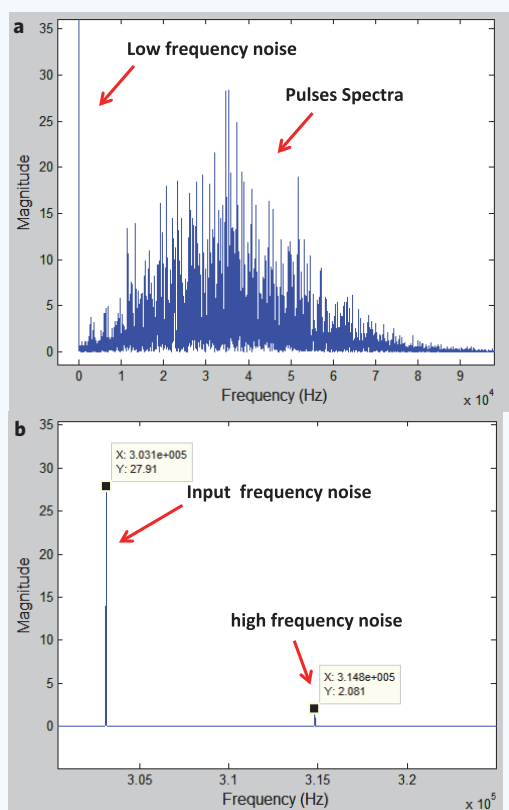
To validate the neutrophil count obtained after the skewness analysis, the lysed blood output of the chip is collected and conjugated with florescent CD66b antibody (specific to the neutrophils). The sample is
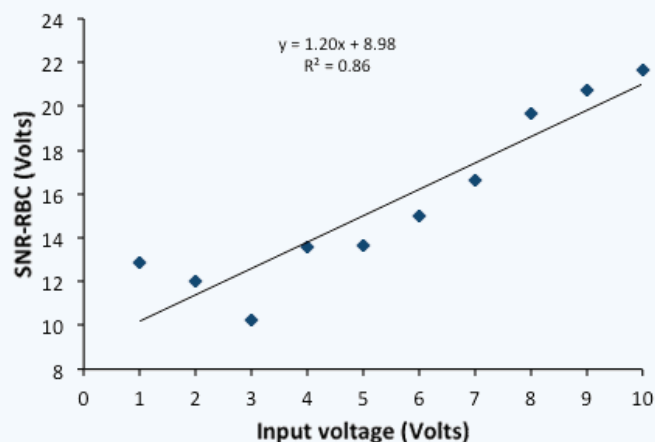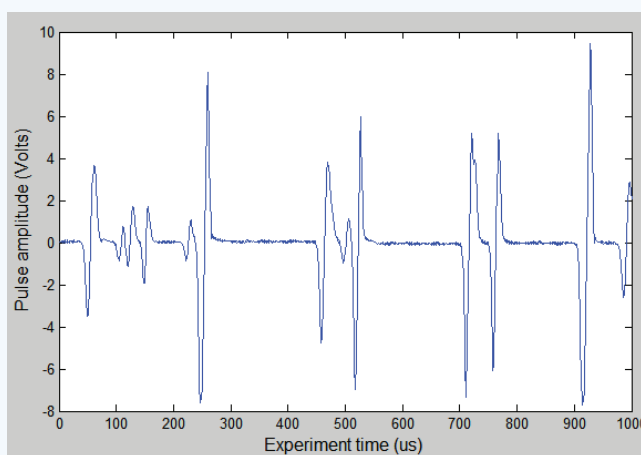
Supplementary Figure 6 The signal-to-noise ratio (SNR) for the pulses corresponding RBCs increases with the increase of the input voltage to the electrodes with $R^2 = 0.86$.
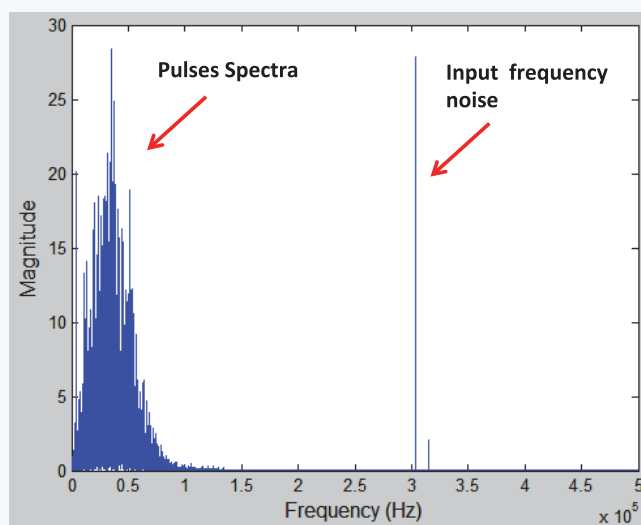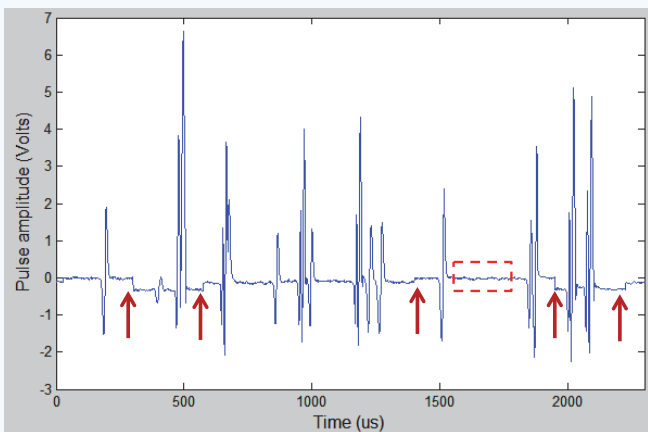

Supplementary Figure 8 Frequency spectrum of the cell counting experiment data after signal filtering. The low-frequency noise in the data is removed by applying a high-pass filter of 20 Hz. To remove the power line frequency, a band-stop filter is used with cut-off frequencies of (58, 62) Hz. The second harmonic of the power line frequency is also removed using a band-stop filter with cut-off frequencies of (118, 122) Hz. The baseline drift is also corrected.

Supplementary Figure 9 Characteristics of a chip for RBC and platelet counting. The voltage pulses obtained as the blood cells pass through the counting channel. The standard deviation of the noise in this case is less than 0.03 V. The baseline shift was removed after the filtering and baseline correction algorithm.
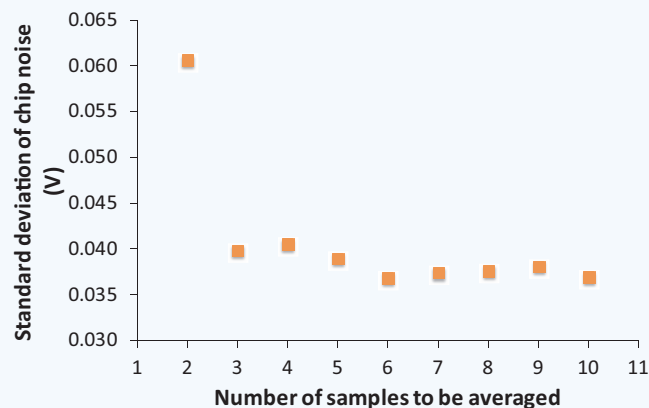
Supplementary Figure 7 Frequency spectrum of the cell counting experiment data before any signal filtering. (**a**) There is low-frequency noise in the data because of the baseline drifts, electronic noise and power line interference (60 Hz). Most of the cell pulses spectrum lies in the range of 5–90 kHz. (**b**) There is an input frequency noise of 303 kHz and another high-frequency noise at 314.8 kHz. These can be removed by using a low-pass filter with cut-off-frequency less than 303 kHz.

Supplementary Figure 10 Characteristics of a chip for RBC counting. The voltage pulses are shown as the blood cells pass through the counting channel. The standard deviation of the noise in this case is greater than 0.05 V (red dotted rectangle). After the filtering and baseline drift correction the baseline still shows a lot of unexplained abrupt changes in the amplitude (shown by red arrows).
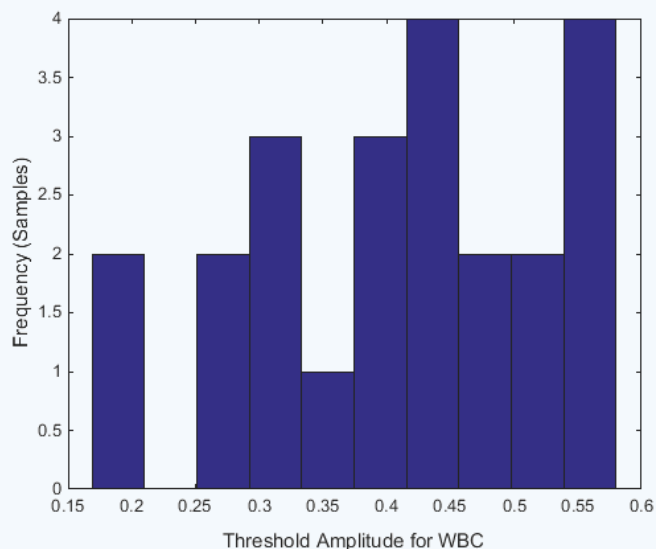

Supplementary Figure 11 The decrease in the standard deviation of the chip noise with signal averaging. Increased number of samples for averaging will result in decreased standard deviation for the chip noise.

incubated and run through the flow cytometer. **Supplementary Fig. 5a** shows the forward *vs.* backscatter plot of the lysed output, which clearly differentiates in between WBCs and debris. In **Supplementary Fig. 5b**, the neutrophil population is gated out and the neutrophil counts were compared with the neutrophil counts obtained from the skewness approach. This analysis is done for three samples and the % errors obtained were 5.2%, 3.7% and 6.1% respectively.

Voltage threshold selection for cell counting

Supplementary Fig. 12 shows the histogram of the voltage threshold values selected for total WBC counting for 22 blood samples experiments. The mean voltage value is 0.41 V with standard deviation of 0.12 V, showing almost 29.2% variability in the threshold. Threshold value is selected manually considering the minima in between debris and lymphocyte population. The variability in the threshold is a result of variability in the fabrication process and experimental noise in the setup in laboratory. In a point-of-care automated cell counter, the threshold selection will be completely automated as the cartridges/electrodes will be mass manufactured and the fabrication process will be more streamlined.

Supplementary Figure 12 Voltage histogram of the selected threshold for total WBC counting.